Active Sensing on a Bicycle for Simultaneous Search and Tracking of Multiple Rear Vehicles

Woongsun Jeon and Rajesh Rajamani

Abstract— This paper uses an inexpensive laser sensor mounted on a rotationally controlled platform to simultaneously search for and track vehicles that are behind a bicycle. Vehicles in the bicycle's lane and in the adjacent left lane are both considered. The tasks involved are searching both lanes to detect presence of vehicles, tracking a vehicle's trajectory once it has been detected, and switching between searching and tracking as needed. A rigorous search algorithm that minimizes the number of sensor rotational angles needed to search the entire region of interest is developed. An error covariance matrix approach is utilized to switch between tracking vehicles and searching the region of interest. Detailed simulation results are presented to show how the developed system handles the absence and presence of vehicles in the two lanes and handles different types of lane change maneuvers while tracking multiple vehicles. Since the developed system uses an inexpensive lightweight sensor that is suitable for on-bicycle implementation, it can be used to detect the danger of a collision and provide a corresponding horn-like audio alert to the motorist.

Index Terms—Smart bicycle, collision warning, collision prevention, vehicle tracking, estimation.

I. INTRODUCTION

BICYCLING is a healthy physical activity for all ages. It can provide both physical and mental health benefits, including reducing the incidence of cancer [1], cutting the risk of heart disease by half [2], postponing Alzheimer's disease [3], [4], and promoting mental alertness and memory [5]. As a form of transportation for commuting to work, bicycling requires no fuel, is three times as efficient as walking, reduces traffic congestion, highly reduces the space needed for parking, and can provide personal cost savings of up to \$8,758 a year compared to owning a typical second car [6]. From 2000 to 2016, the share of people commuting by bicycle has seen 51% growth nationwide, and there were a total of 863,979 bicycle commuters nationwide in 2016 [7].

While bicycle commuting has increased dramatically, very little research resources are currently spent on improving technology for bicycle safety. To the best of this research team's knowledge, only a few research teams and one company have developed sensor systems for bicyclist safety. A magnetometer

This research was supported in part by a research grant from the National Science Foundation (NSF Grant PFI-1631133).

Woongsun Jeon and Rajesh Rajamani are with the Department of Mechanical Engineering, University of Minnesota, Twin Cities, Minneapolis,

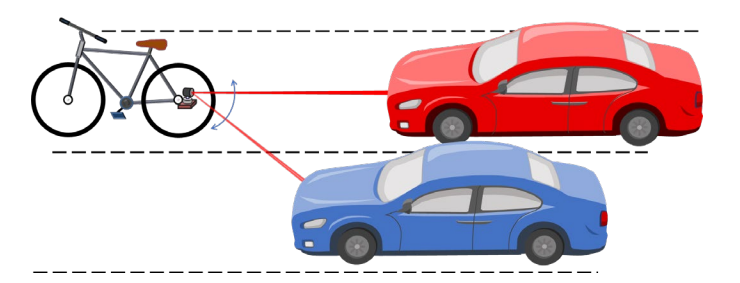


Fig. 1. Multiple vehicle tracking using a laser sensor system on a bicycle.

based system has been developed to identify dangerous locations to bicycles due to heavy automotive traffic [8]. A Rutgers University team has explored a rear-approaching vehicle detection system using computer vision techniques [9]. An undergraduate Northeastern University team explored a sonar sensor system to monitor vehicles at the rear and front of a bicycle [10]. Garmin has developed a rear-collision prevention system using radar [11]. The sensor systems currently explored for bicycles are simplistic, do not estimate car maneuvers or 2-dimensional trajectories and do not require a high-performance processor.

According to the Insurance Institute for Highway Safety, there were 3,300 bicyclist fatalities in bicyclist-motorist crashes in a five-year period and seventy-four percent of the fatalities occurred when the bicyclist was struck by the front of a passenger vehicle [12]. Furthermore, the most common bicyclist-motorist collision scenario involved a vehicle traveling in the same direction as a bicycle and hitting it from behind [13]. This rear bicyclist-motorist collision accounts for 40% of the fatalities [13]. Therefore, a vehicle detection and tracking system for rear vehicles is highly valuable and the system can be used to predict impending collisions and to provide warnings to both the bicyclist and the motorist behind the bicycle. In particular, the collision warning system in this paper will focus on warning the motorist by sounding a loud horn to alert him/her to the presence of the bicycle.

Tracking of multiple rear vehicles (driving right behind the bicycle and in an adjacent lane next to the bicycle), as shown in Fig. 1 is beneficial in order to more reliably prevent accidents by rear vehicles. For example, a vehicle driving in an adjacent lane can change lanes to get behind the bicycle. Then, there may

MN 55455 USA (e-mail: jeonx121@umn.edu; rajamani@umn.edu, TEL: 612-626-7961).

TABLE I
CURRENT SENSOR SYSTEMS EXPLORED FOR BICYCLE SAFETY

Application	Type of detection technology	Cost	Number of identifiable targets/ Field of view (FOV)	Type of notification	Disadvantages
Bicycle Safety System	Radar (Garmin Varia radar [11])	\$300 (with Head unit)	8 targets	Visual	 Tracks only vehicle longitudinal motion. Does not provide audio alert to the motorist.
	Optical (Video camera [9])	\$230 - \$600	FOV: 38° (varies by lens)	Audio	 Limits in weather and lighting conditions. Requires high-performance processors. Alerts only the bicyclist.
Vehicle Safety System	Radar (Delphi adaptive cruise control [14])	\$2,000	64 targets	Visual and Audio	 Too expensive for bicycle application. Difficult to power using batteries on a bicycle.
	Optical (Mobileye [15])	\$850	FOV: 38°	Visual and Audio	 Too expensive for bicycle application. Limits in weather and lighting conditions.
	LIDAR (Google self-driving car [14])	\$75,000	FOV: 360°	Visual and Audio	 Too expensive for bicycle application. Too big, heavy, and difficult to power using batteries on a bicycle.

not be enough time to estimate the vehicle motion or warn the motorist unless the vehicle has been previously tracked. Another possible situation is one which involves a tracked vehicle that changes lane to the adjacent lane from the same lane as the bicycle and then a second vehicle is found to be suddenly approaching right behind the bicycle. In these situations, simultaneous search and tracking of multiple rear vehicles is necessary.

Many automotive researchers use LIDAR, radar or vision systems, or a combination of these sensors and develop tracking algorithms based on each utilized sensor for multiple vehicle tracking [14], [15]. A summary of various technologies from available bicycle and vehicle safety systems is detailed in Table I. Specifically, researchers using expensive high-density LIDARs track multiple vehicles based on measurements from a full scan set of an area of interest [14]. However, these sensors are too big, too expensive, and too difficult to power using batteries on a bicycle. Due to the limitations of a bicycle, we consider utilizing a low-cost single beam laser sensor (\$130) mounted on a rotationally controlled platform [16] for tracking of multiple rear vehicles. Previously, some researches have used the single beam laser sensor for bicycle safety [17 - 19]. However, the developed systems are limited to either the tracking of only a single vehicle behind the bicycle or need additional sensors such as a camera vision system. The laser sensor used in this paper is small and light with low power consumption (less than 130 mA during an acquisition). However, the sensor has only a single laser beam and low sampling frequency (270 Hz typical) [16]. Due to the time needed for rotational platform operation, algorithm processing and data storage, the total sampling frequency will be much lower than the sensor sampling frequency. As a result, the proposed laser sensor system needs too much time to obtain a full scan set of an area of interest.

Therefore, this paper focuses on the development of an intelligent active sensing algorithm for simultaneous search and tracking of multiple rear vehicles based on use of the proposed laser sensor system. We aim to simultaneously monitor and track rear vehicles both in the same lane as the bicycle and in the adjacent lane next to the bicycle, as shown in Fig. 1. The

laser sensor orientation needs to be controlled actively since full scanning is not suitable and too slow for the proposed laser sensor system. Furthermore, the active sensing algorithm requires to deal with not only low sampling frequency of the proposed system, but also a very narrow spread of the laser beam (~8 milli-radians). Since the size of the target (vehicle) is much larger than the spread of the laser beam, a measured point does not provide adequate longitudinal and lateral position of the target vehicle. For instance, either lateral or longitudinal distance between the sensor and vehicle is uncertain unless the measured point is on the exact right corner of the vehicle. In order to overcome the low sampling frequency of the system, an efficient search method is proposed by defining discretized regions of the search area. A Truncated Interacting Multiple Model (Truncated IMM) estimator is proposed to estimate vehicle motion via measurements from the narrow single beam laser sensor. Active sensor control method based on a minimization of search area uncertainties and vehicle position uncertainties is proposed for simultaneous search and tracking of rear vehicles.

This paper is organized as follows. In Section II, a brief review of the work on the tracking of a single rear vehicle together with experimental results is provided and the challenges with multiple rear vehicle tracking are discussed. In Section III, an efficient search method by discretized regions of search area and uncertainty minimization is proposed. Vehicle motion tracking using a Truncated IMM is proposed in Section IV. Then in Section V, active sensor orientation control strategy for simultaneous search and tracking by minimization of uncertainties is proposed. Results of simulation studies and discussions are presented in Section VI. Conclusions are presented in Section VII.

II. CHALLENGES WITH TRACKING OF MULTIPLE REAR VEHICLES

A. Tracking of a Single Rear Vehicle

The sensor system on a bicycle is required to be inexpensive, small and lightweight. In order to meet these constraints, we use a low-cost single beam laser sensor mounted on a rotationally controlled platform for tracking of a rear vehicle. Since the laser

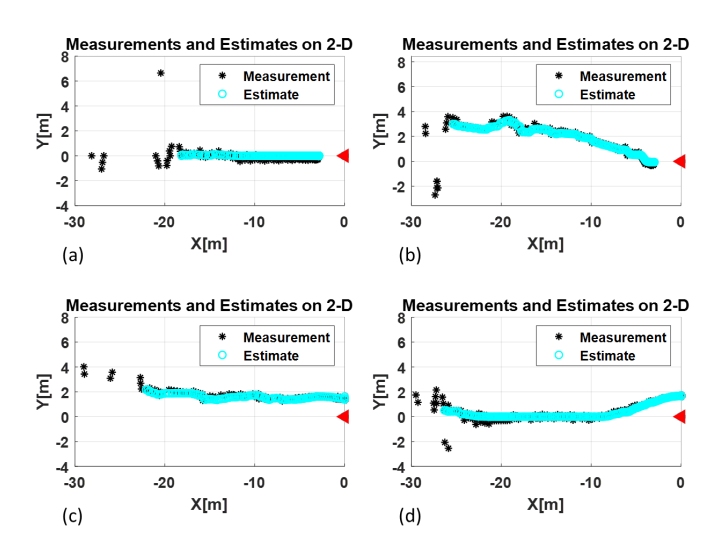


Fig. 2. Experimental results of rear vehicle tracking (red triangle: bicycle). (a) A vehicle approaching right behind, (b) A vehicle changing lane to the right, (c) A vehicle passing by bicycle, and (d) A vehicle changing lane to the left.

sensor can only measure one reflection at a time, the rotational orientation of the laser sensor is required to be controlled in real-time to continuously focus on the tracked vehicle, as the vehicle's lateral and longitudinal distances keep changing.

If it is assumed that there is only one vehicle behind the bicycle, then a control system for tracking a single vehicle using the laser sensor was demonstrated in [17]. The active sensing algorithm in [17] used a receding horizon framework for active orientation control of the laser sensor and an interacting multiple model (IMM) framework for vehicle state estimation.

The previous estimation and control systems are presented here in brief before we discuss the challenge of tracking multiple rear vehicles behind the bicycle using a single laser sensor.

In the IMM framework, the constant velocity model and the nearly coordinated turn model [20] are used for straight motion and turning motion respectively. The state vector is

$$X = [x \quad y \quad v \quad \theta \quad \omega]^T \tag{1}$$

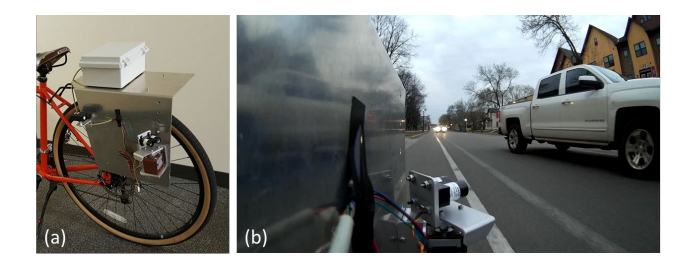
where (x, y), v, θ , and ω are the vehicle position in Cartesian coordinates, speed, orientation, and turn rate in sensor body frame. The discrete-time state space equation for the constant velocity model is given by

$$X_{k+1} = \begin{bmatrix} x + v\Delta T \cos \theta \\ y + v\Delta T \sin \theta \\ v \\ \theta \\ 0 \end{bmatrix}_{k} + w_{v,k}$$
 (2)

The discrete-time state space equation for the nearly coordinated turn model is given by

$$X_{k+1} = \begin{bmatrix} x + \frac{2v}{\omega} \left\{ \sin\left(\frac{\omega\Delta T}{2}\right) \cos\left(\theta + \frac{\omega\Delta T}{2}\right) \right\} \\ y + \frac{2v}{\omega} \left\{ \sin\left(\frac{\omega\Delta T}{2}\right) \sin\left(\theta + \frac{\omega\Delta T}{2}\right) \right\} \\ \theta + \omega\Delta T \\ \omega \end{bmatrix} + W_{c,k}$$
 (3)

where ΔT is the sampling time, and w is the process noise. Each process noise is assumed to be zero mean with covariance as



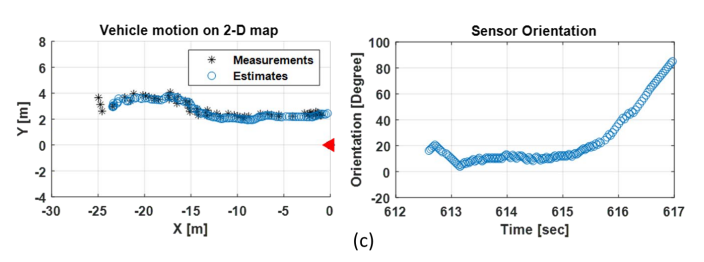


Fig. 3. Sensor implementation and experimental results. (a) Laser sensor system on a bicycle, (b) A screenshot of experimental video, and (c) Experimental results of on-road test with the laser sensor (red triangle: bicycle).

$$Q_{v,k} = diag \begin{bmatrix} \sigma_{vx}^2 & 0\\ 0 & \sigma_{vy}^2 \end{bmatrix}, \Delta T^2 a_{a1}^2, \begin{bmatrix} 0 & 0\\ 0 & 0 \end{bmatrix}$$
(4)

and

$$Q_{c,k} = diag \begin{bmatrix} \sigma_{vx}^2 & 0 \\ 0 & \sigma_{vy}^2 \end{bmatrix}, \Delta T^2 a_{a2}^2, \begin{bmatrix} \Delta T^3 a_{\omega}^2/3 & \Delta T^2 a_{\alpha}^2/2 \\ \Delta T^2 a_{\alpha}^2/2 & \Delta T^2 a_{\alpha}^2 \end{bmatrix}$$
e vehicle motion estimation, the IMM operates ty

For the vehicle motion estimation, the IMM operates two extended Kalman filters (EKF) using the models in (2) and (3) in parallel, and computes state and estimates using suitable mixing of the estimates and covariance from the two models.

The receding horizon controller determines the optimal control input to the sensor based on predicted future vehicle motion under control input constraints:

$$u_k^* = \begin{cases} \arg\min_{u_k} \left\| \frac{\hat{y}_{k+1} + \delta_y}{\hat{x}_{k+1}} - \tan(\phi_k + u_k) \right\|^2, \\ \text{if longitudinal distance is desired} \\ \arg\min_{u_k} \left\| \frac{\hat{y}_{k+1}}{\hat{x}_{k+1} + \delta_x} - \tan(\phi_k + u_k) \right\|^2, \\ \text{if lateral distance is desired} \\ \text{subject to} \quad \hat{x}_{k+1} = f_{1,k}(X_k), \ \hat{y}_{k+1} = f_{2,k}(X_k), \\ \hat{x}_{k+1} > 0, \end{cases}$$

 $u_k \in U$, $\phi_{min} \le \phi_k + u_k \le \phi_{max}$

where $f_1(\cdot)$ and $f_2(\cdot)$ are the vehicle motion model which corresponds to x and y respectively, δ_x and δ_y are distance margins which are used to construct reference points on the target vehicle, U is a finite set of feasible control inputs and ϕ_k is the sensor orientation at time k. By using (6), we track the right front corner (x,y) of the target vehicle by measuring alternately distances to the front and side of the vehicle at points close to the right front corner. Therefore, the reference point for orientation control is changed alternately depending on the corresponding selection of which information (longitudinal or lateral) is needed. The predicted vehicle motion $(\hat{x}_{k+1}, \hat{y}_{k+1})$ is calculated in the IMM framework, as described in [17].

B. Experimental Results

The active sensing algorithm was successfully demonstrated for tracking any single rear approaching vehicle [17]. As shown in Fig. 2, it is shown that the low-cost single beam laser sensor can be used to detect and track a rear vehicle in situations that are commonly encountered with respect to rear vehicles and bicycles: i) a vehicle approaching right behind a bicycle, ii) a rear vehicle with a lateral offset initially going straight and then changing lanes to the right, iii) a rear vehicle with a lateral offset passing by a bicycle, and iv) a vehicle right behind a bicycle and then changes lanes to the left from behind the bicycle. Also, recent on-road tests with the laser sensor system show good performance during both scanning and during tracking of a vehicle, as shown in Fig. 3. For the tests, small size and lowpower consumption microcontroller (Teensy 3.6) operates all the active sensing and tracking algorithm, and data storage. The laser sensor is sucessfully controlled to track the vehicle and obtains measurements continuously. As a result, the laser sensor system estimates vehicle motion well. In this paper, we further develop an active sensing algorithm for tracking of multiple rear vehicles using the laser sensor system.

C. Challenges with Multiple Rear Vehicle Tracking

The single beam laser sensor can measure the distance from only a single reflection and needs to be correctly oriented towards the vehicle whose distance needs to be measured in real-time. Tracking of multiple rear vehicles therefore has multiple challenges compared to tracking of a single rear vehicle. For single vehicle tracking, after target detection, the laser sensor system is only required to continuously focus on the target vehicle. However, in order to track multiple vehicles, a laser sensor system needs to carry out search and multiple vehicle tracking tasks simultaneously. While the sensor system tracks a target vehicle in one lane, searching for a new target vehicle in another lane also needs to be conducted. Therefore, an efficient search method is desired to search for additional rear vehicles. Furthermore, for sensor control, it is necessary to deal with the questions of where to search for a new target vehicle, when to search for a new target vehicle, and which target vehicle to measure at what time among multiple target vehicles. In order to address these problems, we propose an active sensing algorithm for multiple rear vehicle tracking based on a minimization of search area uncertainty and a minimization of vehicle position uncertainty.

III. SEARCHING FOR NEW VEHICLES OF INTEREST

In order to prevent a bicyclist-motorist crash from rear vehicles, vehicles from both right behind the bicycle and from an adjacent lane next to the bicycle will be monitored in this paper.

Hence, three different sensing missions can arise as follows:

1) Search all regions of interest in both lanes to identify new target vehicles, 2) Track one vehicle and search all regions of interest that are not occupied by the tracked vehicle, and 3) Track two vehicles.

In this section, we first show how to conduct the first mission, i.e. how to discretize the search area of both lanes for an

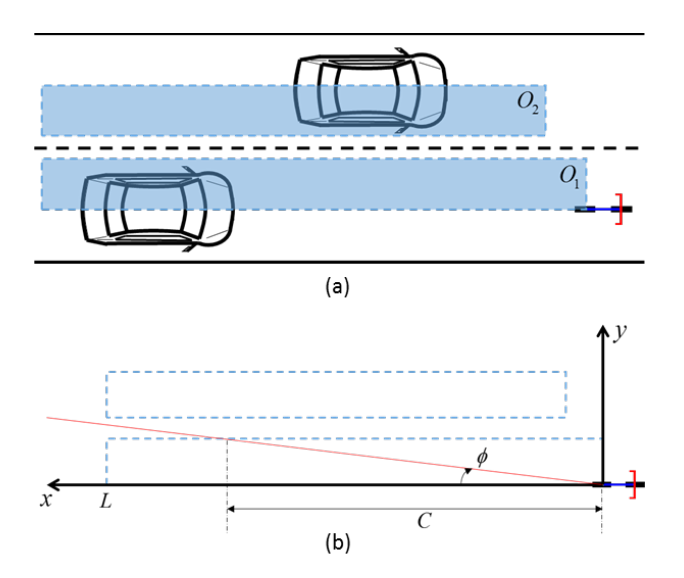
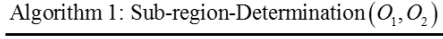


Fig. 4. Search area. (a) Reduced search area, and (b) Longitudinal distance C covered by sensor orientation in bicycle body fixed coordinates.



- 1 $O \leftarrow O_1 \cup O_2$
- 2 Ω←{}
- 3 Γ←{ }
- 4 *i* ←1
- 5 while $O \neq NULL$
- 6 Find ϕ_i such that maximizes C in O
- 7 Define the space covered by ϕ_i as sub-region Ω_i
- 8 $O \leftarrow O \setminus \Omega_i$
- 9 $\Omega \leftarrow \Omega \cup \{\Omega_i\}$
- 10 $\Gamma \leftarrow \Gamma \cup \{\phi_i\}$
- 11 $i \leftarrow i+1$
- 12 return Ω , Γ

efficient search. Then, we discuss a propagation of uncertainties assigned to the discretized regions, and propose a search strategy using these uncertainties.

A. Search Area Discretization for Rear Vehicle Detection

The area to be monitored can be reduced to narrower zones O_1 and O_2 than its lanes since vehicles on roads occupy most lateral space in their lanes, as shown in Fig. 4 (a). Then, the search areas O_1 and O_2 must be further divided into sub-regions for an efficient search. Instead of discretizing each area arbitrarily, a variable C is introduced to define sub-regions. C is the longitudinal distance covered by any specific laser sensor orientation ϕ , as illustrated in Fig. 4 (b). The max lane length C is defined based on the maximum range of the laser sensor. Finally, sub-regions can be defined using the Algorithm 1 table.

Fig. 5 describes how Algorithm 1 works for the situation of two lanes in which the search area is set from 0 to 25m for the lane in which the bicycle is riding, and from 6.25m to 25m for the adjacent lane. First, it is easy to see that C is maximized in the lane right behind the bicycle with the sensor orientation ϕ_1 shown in Fig. 5. The space covered by ϕ_1 is defined as a first

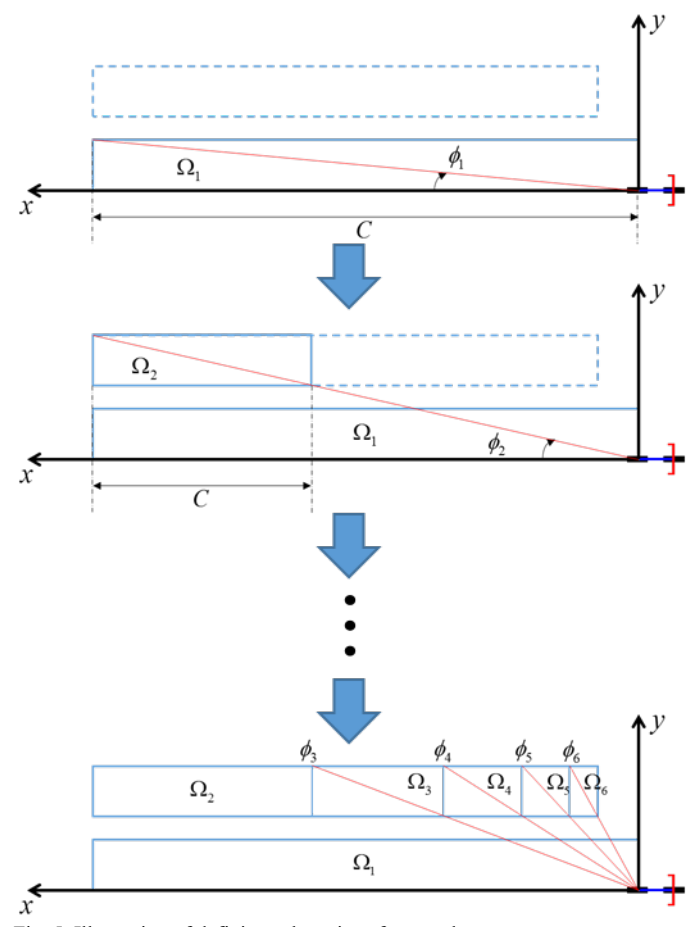


Fig. 5. Illustration of defining sub-regions for search.

sub-region Ω_1 . Then, without considering Ω_1 , C is maximized next with a sensor orientation ϕ_2 as shown in Fig. 5. Similar to the first sub-region case, we define a second sub-region Ω_2 . By doing this iteratively, the search area is discretized into sub-regions Ω_1 , Ω_2 , \cdots Ω_6 .

Lemma 1: If an area of interest is defined as a rectangle, C is maximized when ϕ is chosen so that the laser sensor aims at the top left point of the area of interest.

Proof: Let the minimum and maximum lateral distances, and minimum and maximum longitudinal distances of the rectangular area from a sensor be denoted as (y_{lb}, y_{ub}) , and (L_0, L) . Then, C can be described by two cases that the line of sight of the sensor crosses i) the left edge of the rectangular area, and ii) the top edge of the rectangular area:

$$\begin{cases}
L = \frac{y_{lb}}{\tan \phi}, & \tan^{-1}\left(\frac{y_{lb}}{L}\right) \le \phi \le \tan^{-1}\left(\frac{y_{ub}}{L}\right) \\
\frac{y_{ub}}{\tan \phi} - \frac{y_{lb}}{\tan \phi}, & \tan^{-1}\left(\frac{y_{ub}}{L}\right) \le \phi \le \tan^{-1}\left(\frac{y_{ub}}{L_0}\right)
\end{cases} (7)$$

From (7), C is maximized when ϕ is equal to $\tan^{-1}(y_{ub}/L)$. This implies that ϕ which aims at the top left point of the rectangular area maximizes C at each iteration.

Lemma 2: By applying algorithm 1 successively on the areas of interest O_1 and O_2 in Fig. 4 (a), the residual area 0 is always a single rectangle after each iteration.

Proof: At the first iteration, it is easy to see that maximized

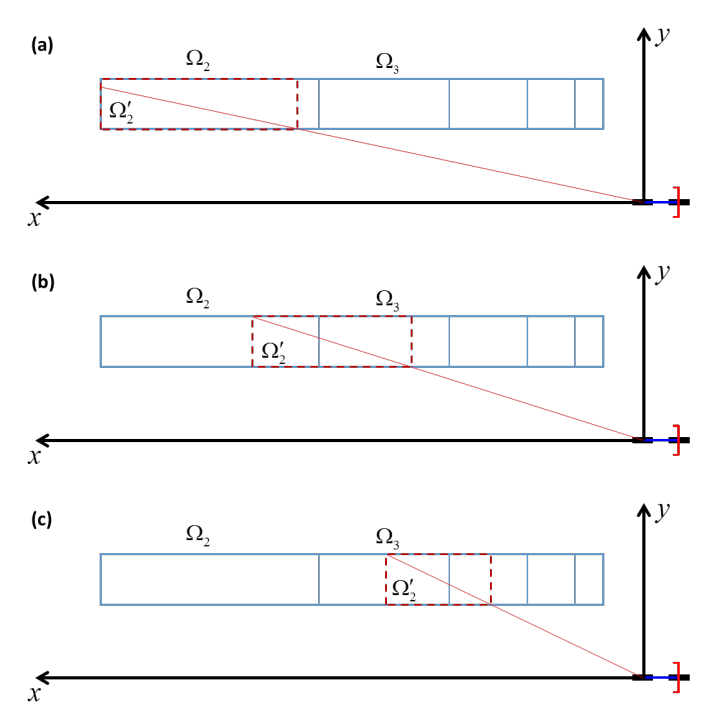


Fig. 6. Cases with $\Omega_2 \neq \Omega_2'$. (a) Ω_2' is entirely overlapped with Ω_2 , (b) Ω_2' is partially overlapped with Ω_2 , and (c) Ω_2' is not overlapped with Ω_2 .

C is same as the longitudinal distance of O_1 . Then, residual area O becomes the same as O_2 which is a single rectangle.

From Lemma 1, Ω_i is always defined from the most left part of 0, and the residual area is always a single rectangle after each iteration.

Theorem 1: Algorithm 1 provides the minimum number of sensor orientations which fully cover the areas of interest O_1 and O_2 in Fig. 4 (a).

Proof: It is straight forward to see that a smaller search area can be covered by less or equal number of sensor orientations compared to a larger search area unless the search area is a set of disconnected areas (Even though the search area is small, more number of sensor orientation may be required if the search area consists of disconnected areas which are far from each other).

Let O_i be defined as the residual area to be covered after i_{th} iteration of Algorithm 1. Also, let O_i' be defined as the residual area to be covered and Ω_i' be defined as the sub-region defined after i_{th} iteration by any arbitrary method. O_i and O_i' decrease monotonically with iterations.

At the first iteration, it is obvious that Algorithm 1 provides the minimum number of sensor orientations (one) which fully cover the area O_1 , as shown in Fig. 5. Let Ω_1 and Ω_1' be identical as O_1 and let us focus on the area O_2 .

Since Algorithm 1 sets the largest possible space to be covered as a sub-region at the second iteration (Lemma 1), O_2 is always less than or equal to O_2' , i.e., $\Omega_2 \geq \Omega_2'$. O_2 is equal to O_2' only if Ω_2 and Ω_2' are identical. If Ω_2 and Ω_2' are identical, we again have the result that O_3 is always less than or equal to O_3' . If Ω_2' is not identical to Ω_2 , three cases need to be considered as shown in Fig. 6:

Case 1: Let us consider the case Ω'_2 is entirely overlapped

with Ω_2 as shown in Fig. 6 (a). Ω_3 is always less than Ω_3' since $\Omega_2' \cup \Omega_3'$ is less than $\Omega_2 \cup \Omega_3$ even if Ω_3' is defined its maximum from Lemma 1.

Case 2: Let us consider the case Ω'_2 is partially overlapped with Ω_2 as shown in Fig. 6 (b). Ω_3 is always less than Ω_3' since i) $\Omega_2' \cup \Omega_3'$ is less than $\Omega_2 \cup \Omega_3$ even though Ω_3' covers all area left to the Ω_2' , and ii) $\Omega_2' < \Omega_2$ and $\Omega_3' < \Omega_3$ if Ω_3' is defined its maximum on the right-side area of the Ω'_2 from Lemma 1.

Case 3: Let us consider the case Ω'_2 is not overlapped with Ω_2 as shown in Fig. 6 (c). Ω_3 is always less than or equal to Ω_3' since $\Omega_2' \leq \Omega_3$ and $\Omega_3' \leq \Omega_2$.

Sequentially, it is always true that

$$O_i \le O_i', \quad \forall i = 1, 2, \cdots$$
 (8)

Hence, Lemma 2 and (8) imply that Algorithm 1 provides the minimum number of sensor orientations which fully cover the area of interest O_1 and O_2 in Fig. 4 (a).

Scanning using the sensor orientations ϕ_1, \dots, ϕ_6 obtained in Fig. 5 enables target vehicle detection via use of a small discrete number of sensing directions that covers all the area of interest. However, we next propose a more general framework, so as to search and track vehicles simultaneously.

It should be noted that full scanning is highly inefficient. A complete scan over the area of interest requires controlling the orientation of the laser sensor from 0 to 33 degrees. Hence, full scanning with 1 degree resolution will take more than five times as many samples as the proposed discretized region search method to conduct a search task over the area of interest.

B. Search Strategy using Search Area Uncertainty

Unlike single vehicle tracking, the sensor system is required to search for a second target vehicle while also tracking a first vehicle. We formulate this search problem as an uncertainty minimization problem. Uncertainties S_1, \dots, S_n are assigned to sub-regions $\Omega_1, \Omega_2, \dots \Omega_n$ defined by Algorithm 1 (n is the number of sub-regions). These uncertainties depend respectively on how long ago each region was searched.

Without a search action, the uncertainties of each region keep increasing over time (time update). Once the sensor examines a region, the uncertainty of the region decreases based on fraction of the region searched (measurement update).

The time update for the uncertainty in a specific region [21] is utilized as follows for uncertainty propagation:

$$\underline{S}_{k+1|k} = \underline{A}\underline{S}_{k|k} \tag{9}$$

 $\underline{S}_{k+1|k} = A\underline{S}_{k|k}$ (9) where $\underline{S}_{k|k} = \left[S_{1,k|k}, S_{2,k|k}, \cdots S_{n,k|k}\right]^T$, $A \in \mathbb{R}^{n \times n}$ represents the state transition matrix. A diagonal matrix with elements greater than 1 is simply utilized for the state transition matrix. Therefore, the uncertainties increase as the uncertainties propagate through time. A specific sub-region such as the one right behind a bicycle is required to be monitored more often for the safety of the bicyclist. This can be dealt with by using a larger value of the element corresponding to the specific subregion in the state transition matrix A.

We propose the following measurement update step:

$$S_{i,k+1|k+1} = \left(S_{i,k+1|k}^{-1} + \delta_{i,k}R_{i,k}^{-1}\right)^{-1}, \qquad (10)$$

by modifying the covariance update equation in the Kalman

filter by using the matrix inversion lemma [22].

$$\delta_{i,k} = \begin{cases} 1, & \text{if the region is examined} \\ 0, & \text{otherwise} \end{cases}$$

$$R_{i,k} = e^{\lambda(1 - C_{i,k}/L_i)} \frac{L_i}{C_{i,k}}$$
(12)

$$R_{i,k} = e^{\lambda(1 - C_{i,k}/L_i)} \frac{L_i}{C_{i,k}}$$
(12)

where λ is a positive constant for a penalty when its sub-region is not fully searched. L_i is the full longitudinal distance of the i_{th} sub-region. $C_{i,k}$ is the longitudinal distance covered by the sensor in the i_{th} sub-region at time k. $\delta_{i,k}$ is an indicator if the sensor examines the i_{th} sub-region at time k. Therefore, the uncertainty of a sub-region remains the same as the time update if the sensor does not examine the sub-region ($\delta_{i,k} = 0$). Otherwise, the uncertainty decreases based on the fraction of the sub-region searched $R_{i,k}$. Therefore, the measurement update equation can be used as a cost function to find a best sensor orientation to minimize uncertainties. Also, using the measurement update step, the uncertainty of search area can be updated systematically at any sensor orientation, even while the sensor system tracks a vehicle. The sensor orientation is required to be determined to conduct search task and the uncertainties are used to find which region needs to be searched.

Finally, the search task for control of sensor orientation is done so as to minimize the uncertainty of the entire search area. The following optimization problem is constructed for sensor orientation control:

$$\begin{aligned} u_{s,k}^* &= \arg\min_{u_k} \sum_{i=1}^n \left(\hat{S}_{i,k+1|k}^{-1} + \delta_{i,k} R_{i,k}^{-1} \right)^{-1} + \beta u_k^2 \\ \text{subject to} \quad u_k \in U, \; \phi_k + u_k \in \Phi_k \end{aligned} \tag{13}$$

where $\hat{S}_{i,k+1|k}$ is computed by using the prediction step in (9), β is a weighting factor on input, and Φ_k is a finite set of feasible sensor orientation at time k.

IV. TRACKING OF VEHICLE MOTION

A single beam laser sensor provides limited target vehicle information:

- 1) It is difficult to measure accurately both longitudinal and lateral distances at the same time, unless the laser beam reflects from the exact right front corner position of the vehicle.
- 2) It is also difficult to determine whether the reflected laser beam is from the front or side of the vehicle.

The sensor system is controlled to measure alternately the distances to the front and side near the right front corner of the vehicle to acquire the longitudinal and lateral distances.

In this section, we introduce a finite state machine for the determination of laser beam reflection location. Then, we propose a Truncated IMM estimator to estimate vehicle motion using a single laser measurement. Also, an error covariance matrix from the Truncated IMM is used to define tracked vehicle position uncertainty.

A. Determination of Reflection Location

In order to determine the reflection location of the laser beam, a finite state machine is utilized with two states: A Front state and a Side state, as shown in Fig. 7. The vehicle shape is assumed to be rectangular. Previous and current distance measurements are used for the decision of the state transition.

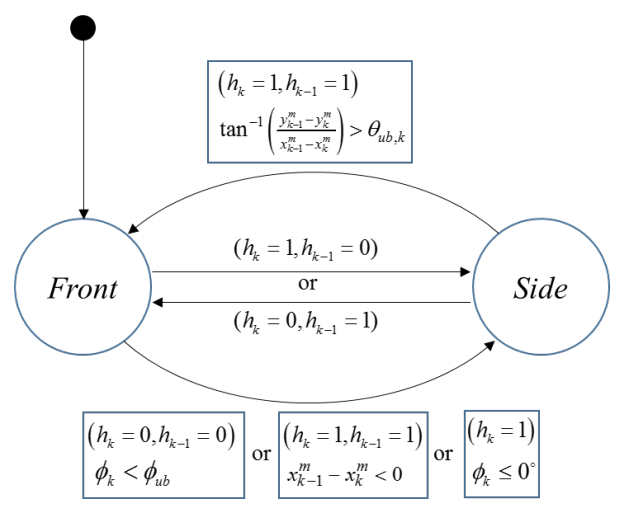


Fig. 7. State diagram for determination of reflection location on a vehicle.

It is noted that every reflection from side or front of the vehicle is not always detectable since it is possible that the incidence angle is too large to reflect enough intensity of the beam to the sensor. Also, it is noted that only one measurement is obtained at a time since the narrow single beam laser sensor is utilized. h_k in Fig. 7 is an indicator on whether the measurement is from the target vehicle or not at time k.

$$h_k = \begin{cases} 1, & \text{if measurement is from vehicle} \\ 0, & \text{otherwise} \end{cases}$$
 (14)

A measurement is assumed to be from the vehicle if the distance between the measurement and estimated vehicle position is within a threshold.

As shown in Fig. 7, the state transition occurs when the measurement is obtained at only one of either current or previous samples. If two measurements are obtained in a row. the decision differs based on the value of the current state. A transition from Front to Side occurs when the subtraction between the projections of the distance measurement to longitudinal axis x_k^m at previous and current time is negative: $x_{k-1}^m - x_k^m < 0$ (15)

$$x_{k-1}^m - x_k^m < 0 (15)$$

A transition from Side to Front is based on the comparison between the slope from two measurements and the estimated orientation of the vehicle

$$\tan^{-1}\left(\frac{y_{k-1}^{m} - y_{k}^{m}}{x_{k-1}^{m} - x_{k}^{m}}\right) > \theta_{ub,k}$$
 (16)

where y_k^m is the projection of the distance measurement to lateral axis and $\theta_{ub,k}$ is sum of estimated vehicle orientation and its error margin at time k. When two measurements are not available in a row, a transition from Front to Side can occur under following condition:

$$\phi_{\nu} < \phi_{\nu h} \tag{17}$$

 $\phi_k < \phi_{ub}$ (17) A left turn maneuver and passing maneuver often lead to a situation where the sensor cannot measure target vehicle position two times in a row. However, a passing maneuver does not require the state transition because the sensor cannot obtain a reflection from the front of the vehicle due to large incidence angle. Condition (17) can distinguish between left turn and passing maneuvers. We set ϕ_{ub} as a maximum incidence angle to reflect enough intensity of laser beam to sensor.

For the situation of a vehicle approaching right behind a bicycle, one additional rule is used for the state transition: The state transition from Front to Side occurs when measurement is obtained with the sensor orientation less than or equal to 0° , and then y_k^m is assumed to be zero. From this, the sensor system tracks the center of a target vehicle when the target vehicle approaches right behind the bicycle. Also, this improves the robustness of the tracking since it is easier to measure the center rather than the right front corner of the vehicle in the situation.

B. Truncated IMM for Vehicle Motion Estimation

Since the spread of the laser beam is very narrow compared to the size of the target vehicle, the laser sensor measurement does not provide adequate spatial information of the target. For example, even if the sensor measures distance from a target vehicle, the measured point can significantly differ from the right corner position of the vehicle. Therefore, it is difficult to estimate both longitudinal and lateral vehicle motion with only a single laser measurement.

For this multiple vehicle tracking problem, we propose a Truncated IMM that combines PDF truncation approach with a IMM estimator. Since the vehicle motion has two distinct maneuvers: straight motion and turning motion, it is difficult to describe the vehicle motion accurately by using only one linear model. Hence, we use two models to describe the vehicle motion and utilize a IMM to estimate the vehicle motion using two models (straight motion and turning motion models). Furthermore, physical constraints on the vehicle motion can be found by using predicted vehicle motion and sensor orientation, in addition to the distance measurement. In order to incorporate the constraints, PDF truncation is utilized with the IMM. The use of PDF truncation also provides better (truncated) error covariance of the vehicle motion including a better model of the vehicle position uncertainty. The vehicle position uncertainty is used to control sensor orientation for tracking and to determine whether a tracking task or a search task requires to be conducted. We first introduce the PDF truncation procedure briefly and then discuss the physical constraints in detail.

In the PDF truncation, we truncate pdf which is assumed to be Gaussian at the constraint edges. Then, the state estimation is computed as the mean of the truncated pdf.

Suppose that at time k, we have the state estimate \hat{X}_k with the error covariance P_k and the s scalar state constraints:

$$a_{j,k} \le \varphi_{j,k}^T X_k \le b_{j,k}, \ j = 1, \dots, s$$
 (18)

where $a_{j,k} < b_{j,k}$. This is two-sided constraint on the linear function of the state $\varphi_{i,k}^T X_k$.

We define $\tilde{X}_{j,k}$ as the state estimate after enforcement of the first j constraints of (18), and $\tilde{P}_{j,k}$ as the covariance of $\tilde{X}_{j,k}$. First, we initialize

$$j = 0$$

$$\tilde{X}_{j,k} = \hat{X}_k$$

$$\tilde{P}_{i,k} = P_k$$
(19)

From Schur decomposition of $\tilde{P}_{j,k}$, orthogonal matrix T and diagonal matrix W are obtained:

$$TWT^T = \tilde{P}_{i,k} \tag{20}$$

Gram-Schmidt orthogonalization is utilized to find the orthogonal matrix $\rho \in \mathbb{R}^{n \times n}$ that satisfies

$$\rho W^{1/2} T^T \varphi_{j,k}
= \left[\left(\varphi_{j,k}^T \tilde{P}_{j,k} \varphi_{j,k} \right)^{1/2} \quad 0 \quad \cdots \quad 0 \right]$$
(21)

Now, the following transformation is conducted:

$$\xi_{j,k} = \rho W^{-1/2} T^T (X_k - \tilde{X}_{j,k})$$
 (22)

From (20) - (22), it can be shown that $\xi_{j,k}$ has zero mean and identity covariance matrix. Also, the lower and upper bounds in (18) are transformed as follows:

$$c_{j,k} = \frac{a_{j,k} - \varphi_{j,k}^T \tilde{X}_{j,k}}{\left(\varphi_{j,k}^T \tilde{P}_{j,k} \varphi_{j,k}\right)^{1/2}} \le [1 \quad 0 \quad \cdots \quad 0] \xi_{j,k}$$
 (23)

$$d_{j,k} = \frac{b_{i,k} - \varphi_{j,k}^T \tilde{X}_{j,k}}{\left(\varphi_{j,k}^T \tilde{P}_{j,k} \varphi_{j,k}\right)^{1/2}} \ge \begin{bmatrix} 1 & 0 & \cdots & 0 \end{bmatrix} \xi_{j,k}$$
(24)

Then, after enforcement of the first normalized scalar constraints in (23) and (24), the mean and variance of the transformed state estimate $\xi_{i+1,k}$ are computed as

$$\tilde{\xi}_{j+1,k} = \begin{bmatrix} \nu & 0 & \cdots & 0 \end{bmatrix}^T$$

$$Cov(\xi_{j+1,k}) = diag(\sigma^2, 1, \cdots, 1)$$
(25)

with

$$\nu = \alpha \left[\exp(-c_{j,k}^{2}/2) - \exp(-d_{j,k}^{2}/2) \right]$$

$$\sigma^{2} = \alpha \left[\exp(-c_{j,k}^{2}/2) (c_{j,k} - 2\mu) \right]$$

$$+\nu^{2} + 1$$
(26)

where

$$\alpha = \frac{\sqrt{2}}{\sqrt{\pi} \left[\operatorname{erf} \left(d_{j,k} / \sqrt{2} \right) - \operatorname{erf} \left(c_{j,k} / \sqrt{2} \right) \right]}$$
 (27)

and error function $erf(\cdot)$ is defined as

$$\operatorname{erf}(t) = \frac{2}{\sqrt{\pi}} \int_0^t \exp(-\zeta^2) \, d\zeta \tag{28}$$

By taking the inverse of the transformation of (22), we obtain the mean and variance of the state estimate which first constraint is enforced:

$$\tilde{X}_{j+1,k} = TW^{1/2} \rho^T \tilde{\xi}_{j+1,k} + \tilde{X}_{j,k} \tilde{P}_{j+1,k} = TW^{1/2} \rho^T Cov(\xi_{j+1,k}) \rho W^{1/2} T^T$$
(29)

After repeating the process above s times $(j = 1, \dots, s)$, we obtain the final constrained state estimate and covariance:

$$\begin{split} \widetilde{X}_k &= \widetilde{X}_{s,k} \\ \widetilde{P}_k &= \widetilde{P}_{s,k} \end{split} \tag{30}$$

More details for the PDF truncation procedure can be found in [22].

Fig. 8 illustrates the entire procedure of the use of the Truncated IMM-EKF. In the mode-matching filtering step, two models: constant velocity model in (2) and nearly coordinated turn model in (3) are utilized. Measurement update is conducted only for the states when its corresponding measurements are available. The measurement noise is assumed to be zero mean and to have covariances σ_x^2 and σ_y^2 for the longitudinal and lateral distance measurements respectively. More details for the theory behind the IMM can be found in [23].

As mentioned earlier, the physical constraints on the vehicle position can be obtained by using sensor orientation and measured or predicted vehicle motion. Predictions of vehicle

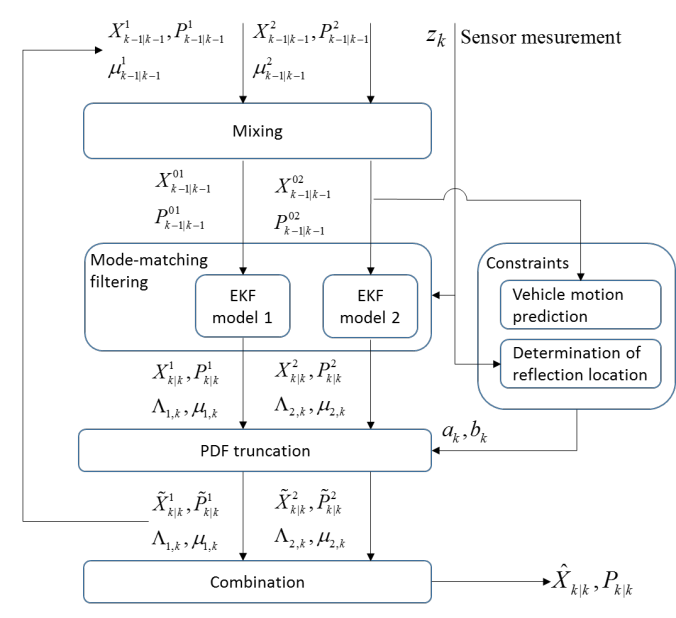


Fig. 8. Overview of vehicle motion estimation using Truncated IMM-EKF.

motion for each mode can be computed by using the initial conditions from Mixing step in Fig. 8 and its models as

$$\hat{X}_{k|k-1}^{l} = f^{l}(\hat{X}_{k-1|k-1}^{0l}), \qquad l = 1, \dots r$$
(31)

where r is the number of modes utilized. Finally, the predicted vehicle motion can be obtained by using mode probability μ :

$$\hat{X}_{k|k-1} = \sum_{l=1}^{r} \hat{X}^{l}_{k|k-1} \mu_{l,k-1}$$
 (32)

Let us consider the case that a laser sensor is controlled to obtain longitudinal distance. If the measurement from the front of the vehicle is available, x is directly updated by using x_k^m . The lateral position of the vehicle is bounded by the line of sight of laser sensor, as shown in Fig. 9. Then, PDF truncation for y is conducted by using bounds:

$$\begin{cases}
 a_k = \hat{y}_{k|k-1} - \gamma_y |\hat{y}_{k|k-1} - y_k^m| \\
 b_k = \hat{y}_{k|k-1} + \gamma_y |\hat{y}_{k|k-1} - y_k^m|
\end{cases}$$
(33)

where γ_{ν} is a positive weight in (0, 1] for reducing lateral vehicle position uncertainty. For the case when lateral distance is measured, we conduct PDF truncation for x using \hat{x}_k and

$$\begin{cases} a_k = \hat{x}_{k|k-1} - \gamma_x |\hat{x}_{k|k-1} - x_k^m| \\ b_k = \hat{x}_{k|k-1} + \gamma_x |\hat{x}_{k|k-1} - x_k^m| \end{cases}$$
 where γ_x is a positive weight in $(0, 1]$ for reducing longitudinal

vehicle position uncertainty.

If the measurement is not available due to large incident angle of laser beam, we can still obtain reasonable bounds using predicted vehicle motion. Unlike the case when measurement is available, we conduct PDF truncation for x (or y) when laser sensor aims at front (or side). The large incident angle leads to tighter bound for the state. Furthermore, x_k^m and y_k^m in (33) and (34) are replaced to x_k^{vir} and y_k^{vir} which are defined as

$$\begin{cases} x_k^{vir} = \hat{y}_{k|k-1} / \tan \phi_k \\ y_k^{vir} = \hat{x}_{k|k-1} \tan \phi_k \end{cases}$$
 (35)

Equation (35) is from the information that we know the target vehicle is not located along the line of sight of laser sensor, and is located near the line of sight of laser sensor since the laser

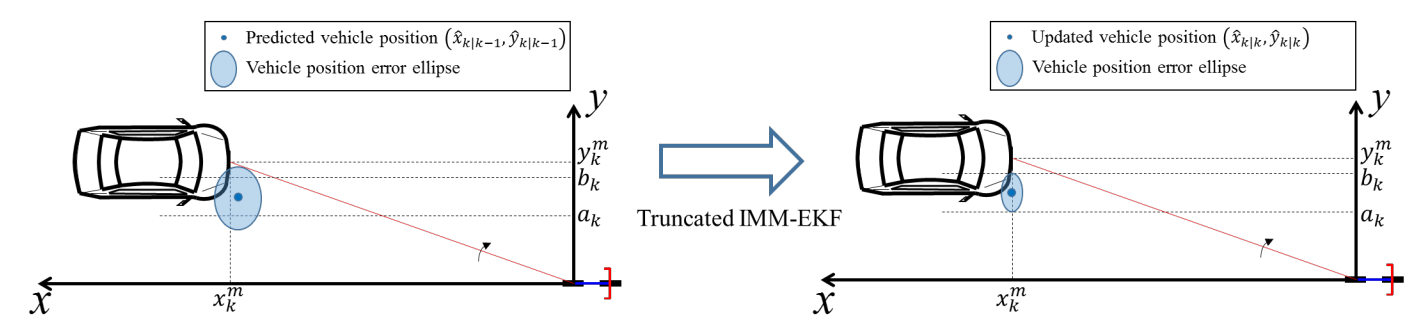


Fig. 9. Illustration of effectiveness of PDF truncation in the case that sensor aims at desired point.

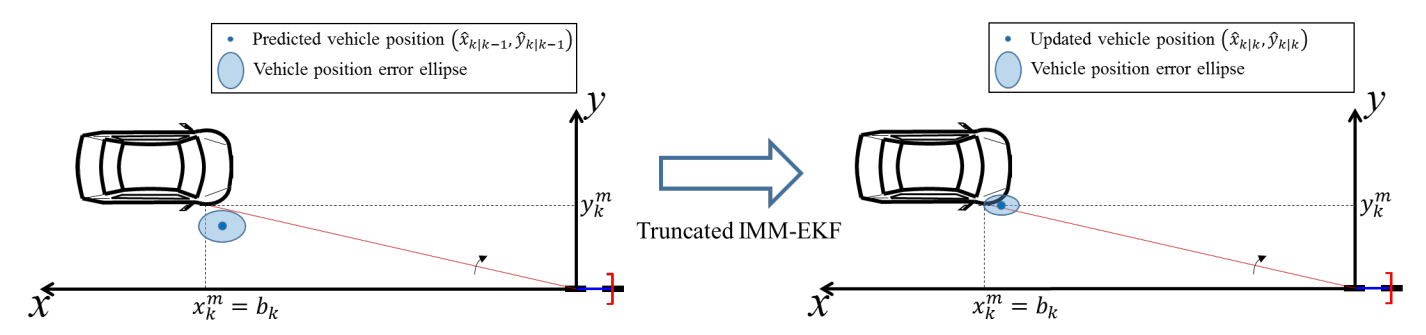


Fig. 10. Illustration of effectiveness of PDF truncation in the case that sensor fails to aim at desired point.

sensor scans near the corner position.

On the other hand, the laser sensor could fail to aim at desired surface of a vehicle due to unexpected vehicle acceleration and steering actions. In this case, PDF truncation is very effective to correct the estimates of vehicle motion. Let us consider the case that a laser sensor is controlled to aim at the front of a vehicle, but the line of sight of the laser sensor is in the side of the vehicle, as shown in Fig. 10. First, larger process noise covariance matrix is used for time update, and then measurement update and PDF truncation conducted as follows. If lateral distance is measured, y is updated by using the measurement and x is corrected by applying PDF truncation with following bounds:

$$\begin{cases}
 a_k = -\infty \\
 b_k = x_k^m
\end{cases}$$
(36)

Similar to the previous case that measurement is not available, PDF truncation is utilized for y instead of x using the following bounds:

$$\begin{cases}
 a_k = y_k^{vir} \\
 b_k = \infty
\end{cases}$$
(37)

If a laser sensor aims at the front of a vehicle even though the sensor is controlled to aim at the side of the vehicle, y_k^m and x_k^{vir} are used for the bounds in (36) and (37) respectively.

V. STRATEGY FOR SIMULTANEOUS SEARCH AND TRACKING

The previous method used for single vehicle tracking in (6) uses predicted vehicle position and fixed small margins δ_x and δ_y to find the sensor orientation control input. It is noted that small margins are utilized to ensure that a laser sensor aims alternately at either front or side of the vehicle, as it is controlled in real-time. However, in the case of multiple vehicle tracking, it is difficult to achieve the same effectiveness using fixed small margins as in a single vehicle tracking. The margins do not take

into account vehicle position uncertainty due to simultaneous search and tracking. The estimated vehicle position often can be different from the actual position in multiple vehicle tracking case due to the intermediate search task. Then, the fixed margin is too small to provide adequate reference points for sensor control to recover tracking performance.

Hence, the use of predicted vehicle position uncertainty is proposed to obtain sensor orientation control inputs, instead of using fixed small margins. We use error covariance matrix to represent the vehicle position uncertainty. First, the Mixing step in Fig. 8 is conducted to compute inputs to each filter from the estimates and covariance from each of the filters at the previous iteration. Then, time update is conducted in each mode, and predicted estimates and predicted error covariance are computed as follows:

$$\hat{X}_{k+1|k} = \sum_{l=1}^{r} \hat{X}^{l}_{k+1|k} \mu_{l,k}$$
 (38)

$$P_{k+1|k} = \sum_{l=1}^{r} \mu_{l,k-1} \left\{ P_{k+1|k}^{l} + \left[\hat{X}^{l}_{k+1|k} - \hat{X}_{k+1|k} \right] \right] \hat{X}^{l}_{k+1|k} - \hat{X}_{k+1|k} \hat{X}^{l}_{k+1|k}$$
(39)

Vehicle position error covariance $\bar{P}_{k+1|k}$ consists of elements corresponding the position of the vehicle in $P_{k+1|k}$. κ -sigma error ellipse is obtained from $\bar{P}_{k+1|k}$ easily by using singular value decomposition. Finally, as shown in Fig. 11, two reference orientations $\phi^{lb}_{ref,k+1}$ and $\phi^{ub}_{ref,k+1}$ for orientation control can be computed analytically from tangent lines to the error ellipse:

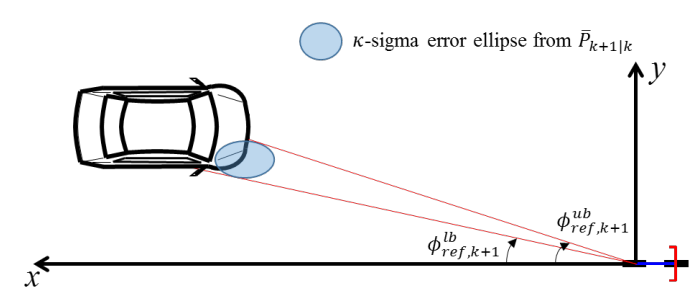


Fig. 11. Reference sensor orientations from vehicle position error covariance.

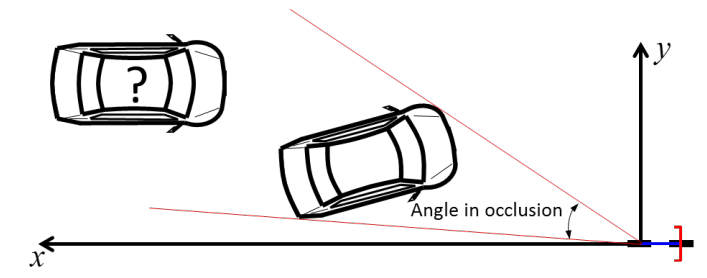


Fig. 12. Occlusion situation.

$$u_{t,k}^{*} = \begin{cases} \underset{u_{k}}{\operatorname{arg \, min}} \left\| \phi_{ref,k+1}^{ub} - (\phi_{k} + u_{k}) \right\|^{2}, \\ \text{if longitudinal distance is desired} \\ \underset{u_{k}}{\operatorname{arg \, min}} \left\| \phi_{ref,k+1}^{lb} - (\phi_{k} + u_{k}) \right\|^{2}, \\ \text{if lateral distance is desired} \\ \text{subject to } u_{k} \in U, \\ \phi_{k} + u_{k} \in \Phi_{k} \end{cases}$$
 (40)

Then, vehicles are tracked by controlling sensor orientation to alternately obtain longitudinal and lateral distances.

For simultaneous search and tracking, the laser sensor system is controlled to minimize search area and vehicle position uncertainties. We quantify the vehicle position uncertainty using the concept of entropy [24]:

$$H = \frac{1}{2}\log(2\pi e)^2 |\bar{P}_{k+1|k}| \tag{41}$$

If the entropy of the vehicle position uncertainty H is larger than a threshold, a laser sensor system tracks the vehicle using (40) to minimize the vehicle position uncertainty. Laser sensor is controlled to aim at the front and side of the vehicle at least once at the tracking. In the case of tracking multiple target vehicles, the sensor system first tracks a vehicle which has larger H. Otherwise, the laser sensor system is controlled by using (13) to perform search task.

The occlusion situation as shown in Fig. 12 is also considered. The sensor orientation occluded by the vehicle is computed by using estimated vehicle position and orientation. Optimal sensor orientation for search task is computed from the finite set of feasible sensor orientation Φ_k in (13) that the angle in the occlusion is excluded. If the sensor orientation for tracking from (40) is in the occlusion, the sensor system attempts to track another vehicle being tracked or search for a new target.

It is noted that the search area uncertainty is always updated by using (10) - (12) whether the sensor system is controlled for search or tracking.

VI. SIMULATION STUDIES AND DISCUSSIONS

Detailed simulation studies are conducted to verify the proposed active sensing algorithm for multiple rear vehicle tracking. In this simulation study, we aim to search and track vehicles in the lane in which the bicycle is riding and also in an adjacent lane next to the bicycle, as shown in Fig. 1.

Fig. 13 shows animation screenshots in simulation studies of three scenarios which require simultaneous search and tracking:

- 1) First car is driving in adjacent lane. Afterwards, second car appears and is driving in the same lane as bicycle.
- 2) First car is driving in the same lane as bicycle and then changes lane to the left. Second car was behind the first

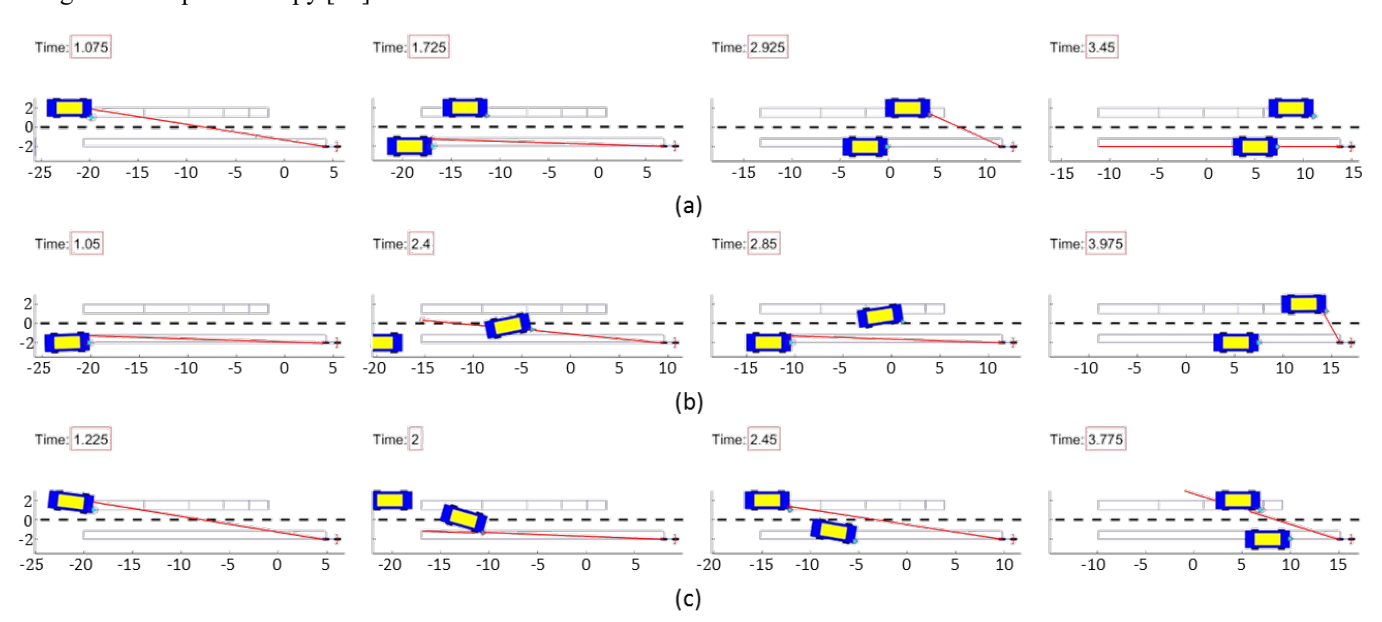


Fig. 13. Animation screenshot in time sequence. (a) Two straight moving vehicles, (b) A left-lane change and a straight moving vehicle, and (c) A right-lane change and a straight moving vehicle.

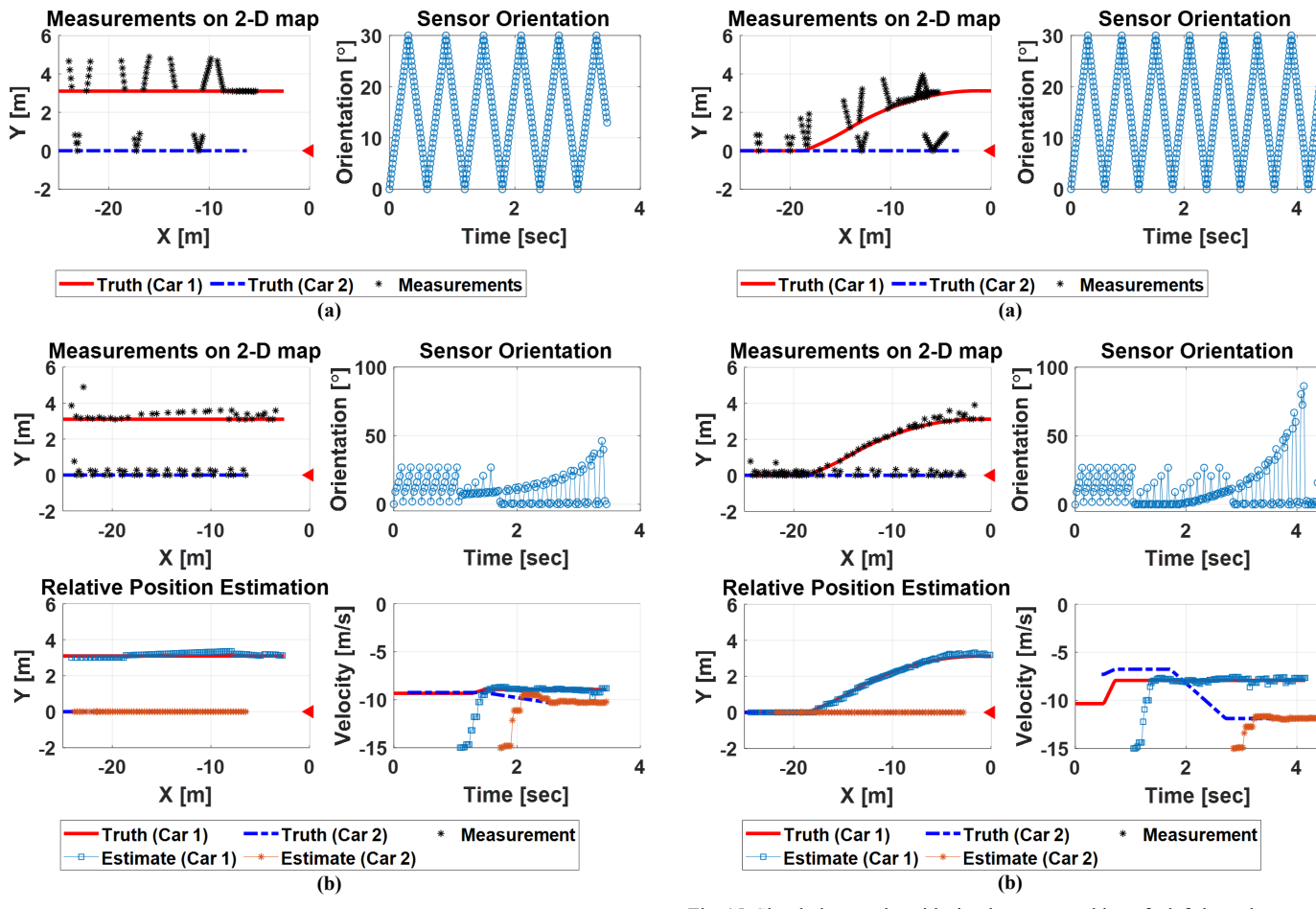


Fig. 14. Simulation results with simultaneous tracking of two straight moving vehicles (red triangle: bicycle). (a) Open-loop scanning with 30 degrees, and (b) Proposed active sensing algorithm using truncated IMM-EKF.

car and now goes straight towards the bicycle, and

3) First car is driving in adjacent lane and then changes lane to the right. Second car was behind the first car and now goes straight in the adjacent lane.

Both vehicles need to be tracked in all scenarios. The function fmincon in MATLAB Optimization Toolbox is used to solve the optimization problem for the search task. Search region is set from 0 to 25m for the lane which bicycle is riding, and from 6.25m to 25m for the adjacent lane. However, the sensor system tracks vehicles in the entire region from 0m to 25m in both lanes. Once tracked vehicle is located in a subregion, R_i of its sub-region and of sub-regions behind the vehicle are set to 0.1 unless the vehicle changes lane. The sensor system stops tracking when the target vehicle passes the bicycle. The incidence angle of a laser beam to objects is considered in this simulation. A value of 70 degrees which is obtained from experiments is utilized as a threshold for maximum incident angle to reflect enough intensity of the beam to the sensor. Gaussian noise $\sim \mathcal{N}(0,2^2 [cm])$ is added to the distance measurements. 2-sigma error ellipse is utilized for tracking problem in (40). γ_x and γ_y are set as 0.5 and 0.7 respectively. We set the value of 7 as a threshold for entropy of the vehicle position uncertainty in (41). For estimation using IMM, the following process and measurement noise

Fig. 15. Simulation results with simultaneous tracking of a left-lane change and a straight moving vehicle (red triangle: bicycle). (a) Open-loop scanning with 30 degrees, and (b) Proposed active sensing algorithm using truncated IMM-EKF.

covariances are utilized: σ_{vx} = 3, σ_{vy} = 5, σ_{a1} = 2000, σ_{a2} = 1000, σ_{ω} = 0.2, σ_{α} = 0.3, σ_{x} = 15 and σ_{y} =15. For IMM, following mode transition matrix is used:

$$\begin{bmatrix} 0.99 & 0.01 \\ 0.01 & 0.99 \end{bmatrix} \tag{42}$$

The bicycle is moving with a constant speed of 4m/s. The initial conditions for Truncated IMM-EKF are set as

$$[x_0 \quad y_0 \quad v_0 \quad \theta_0 \quad \omega_0]^T$$

$$= [x_k^m \quad 0 \quad -15m/s \quad 0 \quad 0.001]^T$$
(43)

if a vehicle is detected at time k in the same lane as bicycle, and

$$[x_0 \quad y_0 \quad v_0 \quad \theta_0 \quad \omega_0]^T = [x_k^m \quad 3m \quad -15m/s \quad 0 \quad 0.001]^T$$
 (44)

if a vehicle is detected at time k in adjacent lane.

First, we conduct simulation studies using an open-loop fixed scan range (30 degrees). The sampling frequency of these simulations is 100 Hz. Fig. 14 (a), 15 (a), and 16 (a) show that vehicle measurements are not available most of the time during open-loop scanning, even though high sampling frequency (100 Hz) and a small scan range (30 degrees) are utilized.

Simulation studies using the proposed active sensing algorithm is conducted, as shown in Fig. 14 (b), 15 (b) and 16 (b). Lower sampling frequency (40 Hz) is utilized to show the far superior effectiveness of the proposed active sensing

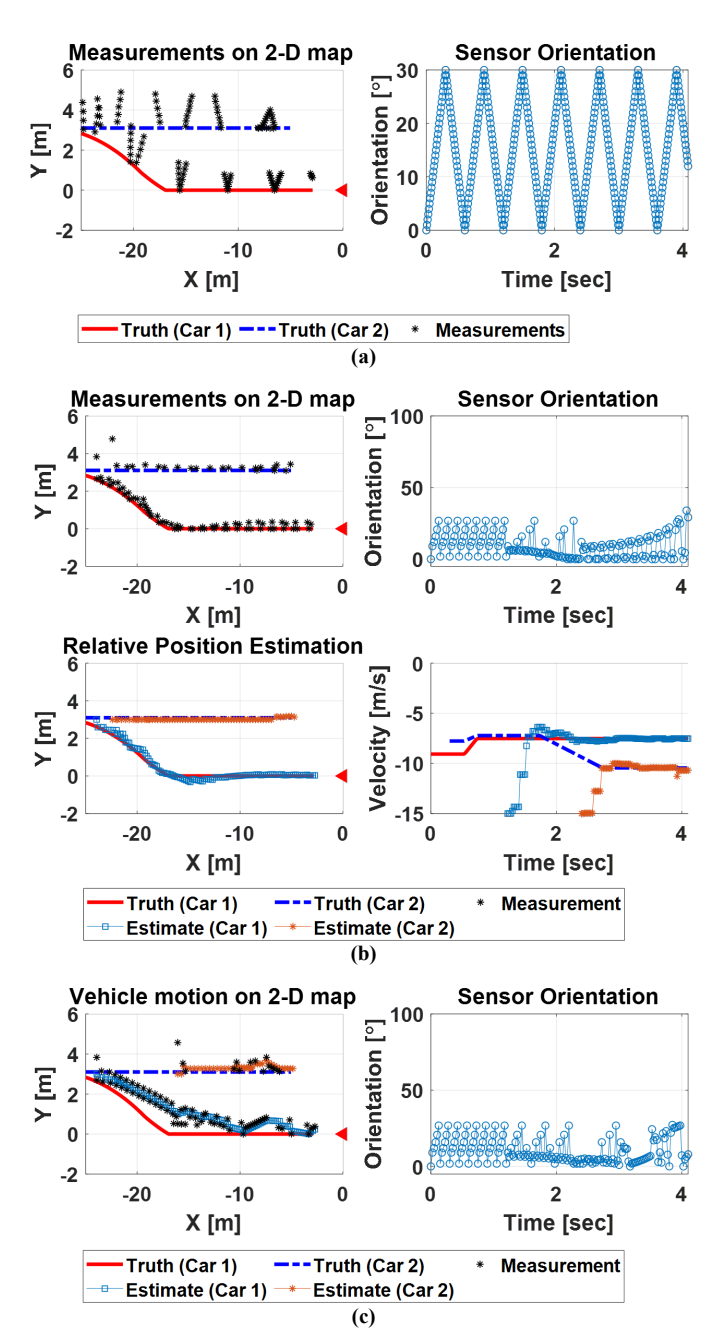


Fig. 16. Simulation results with simultaneous tracking of a right-lane change and a straight moving vehicle (red triangle: bicycle). (a) Open-loop scanning with 30 degrees, (b) Proposed active sensing algorithm using truncated IMM-EKF, and (c) Proposed active sensing algorithm using Kalman filter.

algorithm compared to the open-loop scanning with higher sampling frequency (100 Hz). As shown in Fig. 14 (b), 15 (b) and 16 (b), the sensor system successfully tracks vehicles in the same lane as bicycle and in adjacent lane during straight maneuver and turning maneuvers. The active sensing algorithm obtains measurement data continuously and provides good estimates of vehicle motions. Also, the results verify that the sensor system conducts simultaneous search and tracking, and estimates vehicle motions accurately.

Simulation studies for the senario 3) using a standard Kalman filter are also conducted to demonstrate superiority of the proposed truncated IMM technique, as shown in Fig. 16 (c). For

the Kalman filter, the constant velocity model with Cartesian velocity is used and is given by

$$\begin{bmatrix} x \\ y \\ v_x \\ v_y \end{bmatrix}_{t+1} = \begin{bmatrix} 1 & 0 & \Delta T & 0 \\ 0 & 1 & 0 & \Delta T \\ 0 & 0 & 1 & 0 \\ 0 & 0 & 0 & 1 \end{bmatrix} \begin{bmatrix} x \\ y \\ v_x \\ v_y \end{bmatrix}_{t} + w_{r,k}$$
(45)

where v_x and v_y are the longitudinal and lateral velocities, and $w_{r,k}$ is white noise with covariance as

$$Q_{r,k} = \begin{bmatrix} \sigma_{vx}^{2} & 0 & \frac{\Delta T^{3} \sigma_{ax}^{2}}{2} & 0\\ 0 & \sigma_{vy}^{2} & 0 & \frac{\Delta T^{3} \sigma_{ay}^{2}}{2}\\ \frac{\Delta T^{3} \sigma_{ax}^{2}}{2} & 0 & \Delta T^{2} \sigma_{ax}^{2} & 0\\ 0 & \frac{\Delta T^{3} \sigma_{ay}^{2}}{2} & 0 & \Delta T^{2} \sigma_{ay}^{2} \end{bmatrix}$$
(46)

We set σ_{av} and σ_{av} as same as σ_{al} and $\sigma_{al}/10$. The proposed sensor orientation control algorithms with the same parameters are used for simulation studies, except the value of the threshold for entropy of the vehicle position uncertainty in (41). Since the Kalman filter does not incorporate the physical constraints on the vehicle motion and utilizes a single model, the vehicle position uncertainty is not reduced effectively compared to the truncated IMM-EKF. As a result, the value of 7 as the threshold for entropy is too small, i.e., the sensor system does not conduct search task once the sensor tracks the first vehicle. Thus, we set the value of 8 as a threshold for the entropy in simulation studies. As shown in Fig. 16 (b) and Fig. 16 (c), the sensor orientation control algorithm with the proposed truncated IMM-EKF provides better measurement data close to the corner position and provides better estimation performance compared to the algorithm with the Kalman filter.

If the vehicle performs an extreme left turn maneuver in which acceleration and turn rate are very high, then the active sensing system can lose track of the left turning vehicle. However, in this situation, the active sensing system quickly starts to re-search and can detect the vehicle. The active sensing system terminates tracked vehicle if measurements are not obtained consecutively or vehicle position uncertainty becomes too large. The active sensing system always achieves robust tracking performance for vehicles changing lane to the same lane as the bicycle and for vehicles approaching right behind the bicycle which are significant with regard to bicyclist's safety. These vehicle maneuvers can be tracked using smaller sensor orientation change and the front of the vehicle during the maneuvers is always detectable.

VII. CONCLUSIONS

This paper showed how an inexpensive laser sensor mounted on a rotationally controlled platform could be used to simultaneously search for and track multiple vehicles that are behind a bicycle. Vehicles in the bicycle's lane and in the adjacent left lane were both considered. The tasks involved included searching both lanes to detect presence of vehicles, tracking a vehicle's trajectory once it has been detected, and switching between searching and tracking as needed. A rigorous search algorithm that minimized the number of sensor rotational angles needed to search the entire region of interest

was developed. An error covariance matrix approach was utilized to switch between tracking vehicles and searching the region of interest. Detailed simulation results were presented to show how the developed system handles the absence and presence of vehicles in the two lanes and handles different types of lane change maneuvers while tracking multiple vehicles. Since the developed system uses an inexpensive lightweight sensor, it is very suitable for on-bicycle implementation and can reliably protect the bicycle from rear vehicle collisions by predicting impending collisions and providing a warning in the form of a loud horn to the motorist behind the bicycle.

REFERENCES

- [1] S.G. Wannamathee, A.G. Shaper and M. Walker, "Physical Activity and Risk of Cancer in Middle-Aged Men," *British Journal of Cancer*, Vol. 85, No. 9, pp. 1311-1316, 2001.
- [2] K.R. Wilund, "Is the Anti-Inflammatory Effect of Regular Exercise Responsible for Reduced Cardiovascular Disease?" *Clinical Science*, Vol. 112, No. 11, pp. 543-555, 2007.
- [3] J. Marx, "Preventing Alzheimers: A Lifelong Commitment?" Science, Vol. 309, August 2005.
- [4] S. Balsamo S, J.M. Willardson, S.S. Frederico, J. Prestes, D.C. Balsamo, C.N. da Dahan, L. Dos Santos-Neto, and O.T. Nobrega, "Effectiveness of exercise on cognitive impairment and Alzheimer's disease," *International* journal of general medicine, 6, 387-91 PMID: 23737675, 2013.
- [5] B. Nanda, J. Balde and S. Manjunatha, "The Acute Effects of a Single Bout of Moderate-Intensity Aerobic Exercise on Cognitive Functions in Heathy Adult Males," *Journal of Clinical Diagnostic Research*, Vol. 7, No. 9, 2013.
- [6] M. Woodruff, "Thirteen Reasons You Should Start Biking to Work," Business Insider, Oct 29, 2012.
- [7] K. McLeod, E. Murphy and P. Halupka, "Where We Ride: An Analysis of Bicycling in American Cities," League of American Bicyclists, Report, September 2017.
- [8] S. B. Eisenman, E. Miluzzo, N. D. Lane, R. A. Peterson, G-S. Ahn, and A. T. Campbell, "The BikeNet mobile sensing system for cyclist experience mapping," in 5th ACM Conference on Embedded Networked Sensor Systems (SenSys 2007), Sydney, Australia, 2007, pp. 87 - 101.
- [9] S. Smaldone, C. Tonde, V. K. Ananthanarayanan, A. Elgammal, and L. Iftode, "The cyber-physical bike: a step towards safer green transportation," In 12th Workshop on Mobile Computing Systems and Applications, Phoenix, AZ, 2011, pp. 56 61.
- [10] Northeastern University. (2014, Jan. 21). Northeastern students develop 'Smart Bike' tech to curb cycling death [Online]. Available: http://www.bizjournals.com/boston/blog/startups/2014/01/northeasternstudents-develop-smart.html
- [11] Garmin. Varia Rearview Radar. Accessed: Jan. 26, 2019. [Online]. Available: https://buy.garmin.com/en-US/US/p/518151
- [12] Insurance Institute for Highway Safety, "Bicycle crash study could guide design of bicyclist detection system," IIHS, Report, Vol. 50, No. 3, March 31, 2015.
- [13] K. McLeod, and L. Murphy, "Every bicyclist counts," League of American Bicyclists, Report, May 2014.
- [14] A. Mukhtar, L. Xia, and T. B. Tang. "Vehicle detection techniques for collision avoidance systems: A review," in *IEEE Transactions on Intelligent Transportation Systems*, vol. 16, no. 5, pp. 2318-2338, Oct. 2015.
- [15] Mobileye. Mobileye 5 Series. Accessed: Jan. 26, 2019. [Online]. Available: http://www.mobileye.com/en-uk/products/mobileye-5-series/
- [16] Garmin. Lidar-lite. Accessed: Jan. 26, 2019. [Online]. Available: https://buy.garmin.com/en-US/US/p/557294
- [17] W. Jeon and R. Rajamani, "Rear Vehicle Tracking on a Bicycle Using Active Sensor Orientation Control," in *IEEE Transactions on Intelligent Transportation Systems*, vol. 19, no. 8, pp. 2638-2649, Aug. 2018.
- [18] I. Blankenau, D. Zolotor, M. Choate, A. Jorns, Q. Homann, and C. Depcik, "Development of a Low-Cost LIDAR System for Bicycles," No. 2018-01-1051, SAE Technical Paper, 2018.
- [19] W. Jeon and R. Rajamani, "A novel collision avoidance system for bicycles," 2016 American Control Conference (ACC), Boston, MA, 2016, pp. 3474-3479.

- [20] X. Rong Li and V. P. Jilkov, "Survey of maneuvering target tracking. Part I. Dynamic models," in *IEEE Transactions on Aerospace and Electronic Systems*, vol. 39, no. 4, pp. 1333-1364, Oct. 2003.
- [21] L. F. Bertuccelli and J. P. How, "Search for dynamic targets with uncertain probability maps," in 2006 American Control Conference(ACC), Minneapolis, MN, 2006, pp. 737-742.
- [22] D. Simon Optimal state estimation: Kalman, H infinity, and nonlinear approaches. John Wiley & Sons, 2006.
- [23] Y. Bar-Shalom, X. R. Li, and T. Kirubarajan, Estimation with applications to tracking and navigation: theory algorithms and software. John Wiley & Sons, 2004.
- [24] T. M. Cover, and A. T. Joy, Elements of information theory. John Wiley & Sons, 2012.



Woongsun Jeon received the B.S. and M.S. degrees in mechanical engineering from Yonsei University, Seoul, Korea in 2010 and 2012, respectively. Currently he is working toward the Ph.D. degree in mechanical engineering at the University of Minnesota, Twin Cities, Minneapolis, MN, USA. His research interests include sensing, estimation, and control systems.



Rajesh Rajamani obtained his M.S. and Ph.D. degrees from the University of California at Berkeley in 1991 and 1993 respectively and his B.Tech degree from the Indian Institute of Technology at Madras in 1989. Dr. Rajamani is currently Professor of Mechanical Engineering at the University of Minnesota. His active research interests include sensing and estimation for smart mechanical systems.

Dr. Rajamani has co-authored over 140 journal papers and is a co-inventor on 13 patent applications.

He is the author of the popular book "Vehicle Dynamics and Control" published by Springer Verlag. Dr. Rajamani has served as Chair of the IEEE Technical Committee on Automotive Control and on the editorial boards of the IEEE Transactions on Control Systems Technology, the IEEE/ASME Transactions on Mechatronics, and the IEEE Control Systems Magazine. Dr. Rajamani is a Fellow of ASME and has been a recipient of the CAREER award from the National Science Foundation, the 2001 Outstanding Paper award from the journal *IEEE Transactions on Control Systems Technology*, the Ralph Teetor Award from SAE, and the 2007 O. Hugo Schuck Award from the American Automatic Control Council. Several inventions from his laboratory have been commercialized through start-up ventures co-founded by industry executives. One of these companies, Innotronics, was recently recognized among the 35 Best University Start-Ups of 2016 in a competition conducted by the US National Council of Entrepreneurial Tech Transfer.